PERGAMON

International Journal of Solids and Structures 36 (1999) 3661–3676

INTERNATIONAL JOURNAL OF SOLIDS and STRUCTURES

Analysis of shear band instabilities in sintered metals

Pia Redanz, Viggo Tvergaard*

Department of Solid Mechanics Technical University of Denmark, DK-2800 Lyngby, Denmark

Received 16 January 1998, in revised form 4 May 1998

Abstract

For structural components made of sintered metals the porosity may be rather high, and this affects conditions for material failure. A simple model for analysis of shear band development in uniformly strained solids is used here to study the effect of rather high initial porosities on the onset of a material instability. The elastic plastic behaviour of the material is represented by a material model, which combines the Gurson model, relevant to rather low porosities, with the FKM model, developed for high porosity powder compacts. Predictions are shown for various levels of initial porosity and for various levels of initial material imperfections, considering both plane strain and axisymmetric conditions outside the shear band. Also a comparison of localization predictions by the Gurson model, the FKM model and the combined model is presented.

1. Introduction

In the production of complex shaped engineering components sintered metals are used increasingly, due to the ease of processing and good mechanical properties of the final material. The possibility of forming to near net final shape is one of the obvious advantages of the process. A characteristic difference from the result of other production processes is the porosity of the sintered materials, which ranges from zero up to 0.5. Therefore, in analysing the strength of components made of sintered metals, the possibility of a rather high level of porosity must be accounted for. For this reason Redanz et al. (1997) have analysed the stress state and the conditions for the onset of failure near the tip of a deep notch in an elastic-plastic porous solid. It was found in this study that plastic flow localization at the crack tip is an important part of the failure mechanism, as is also typical for crack growth by a ductile mechanism involving the nucleation and growth of voids to coalescence (Needleman and Tvergaard, 1987).

In the study of Redanz et al. (1997) for a deep notch the material was described by either the Gurson model (Gurson, 1977) or the FKM model (Fleck et al., 1992). The latter model assumes

* Corresponding author. Fax: 004545931475; E-mail: famvig@unidhp.uni-c.dk

0020–7683/99/$ - see front matter
PII: S0020–7683(98)00163–2

that the porous material consists of spherical particles bonded perfectly at more or less plastically deformed contact areas. Thus, the FKM model is applicable at rather high porosities, e.g. from a void volume fraction 0.10 up to the limit value 0.36, which corresponds to a dense random packing of equi-sized spheres. The Gurson model represents a porous material, where a plastic matrix contains separated, spherical voids, and this model is more appropriate for low porosities. Furthermore, in a recent numerical study of the cold compaction of metal powder, Redanz (1998) has also made use of a combination of the two models, as originally suggested by Fleck et al. (1992). In this combined model the Gurson model is used at low porosities, the FKM model is used at high porosities, and a linear interpolation between the two models is used in a transition range.

Localization of plastic flow in a shear band can be studied by a relatively simple model problem, where an initial material inhomogeneity is assumed inside a thin, plane slice of material, and the stress states inside and outside this slice of material, respectively, are assumed to remain homogeneous throughout the deformation history (Rice, 1976). Based on the Gurson material model, this formulation was used by Yamamoto (1978) to determine the effect of an inhomogeneous void volume fraction distribution on the onset of localization, and further studies of this type were carried out by Tvergaard (1981) and Saje et al. (1982). The use of the shear band model was extended by Tvergaard (1982a) to also consider the post localization behaviour far beyond the onset of localization, where the behaviour is often mechanically unstable. This extended model has also been used in a number of subsequent studies (Tvergaard, 1982b, 1987; Tvergaard and van der Giessen, 1991) to obtain further understanding of the behaviour in the post localization range. Thus, it was shown by Tvergaard (1982b) that very early localization due to a burst of nucleation, as found by Saje et al. (1982), tends to have little significance for the material behaviour, since this first localization leads only to a small amount of localized straining before the whole specimen starts to deform plastically again.

In the present paper the extended shear band model is used to study effects of localization on failure of components produced by sintering metal. Analyses are made based on the FKM model, the Gurson model, or the combined model; but the focus is mainly on the combined model, which is expected to give a reasonable approximation of the material behaviour over a large range of porosities.

2. Porous material models

The approximate yield condition for a porous material is not only dependent on the yield strength and the stress state in the material but also on the porosity. In the present study the porosity is assumed to be represented by a scalar which gives a yield surface of the form

$$\Phi(\sigma^{ij}, \sigma_{\mathrm{M}}, f) = 0 \tag{1}$$

where σ_{M} is the current yield stress of the matrix material and f is the void volume fraction or porosity. Initiation of plastic yielding occurs when $\Phi = 0$ is reached while $\dot{\Phi} > 0$. During plastic yielding, the consistency condition, $\Phi = 0$, must be fulfilled.

The analysis is based on a convected coordinate Lagrangian formulation of the field equations. The Lagrangian strain tensor is given by $\eta_{ij} = \frac{1}{2}(G_{ij} - g_{ij})$ where G_{ij} and g_{ij} are the metric tensors in

the current and the reference state, respectively, with the determinants G and g. The Lagrangian strain tensor expressed in terms of the displacement components u^i is

$$\eta_{ij} = \tfrac{1}{2}(u_{i,j} + u_{j,i} + u^k_{,i} u_{k,j}) \tag{2}$$

where $(),_j$ denotes the covariant derivative in the reference frame. The relation between the Kirchhoff stress tensor, τ^{ij}, and the Cauchy or true stress tensor, σ^{ij}, is given by $\tau^{ij} = \sqrt{G/g}\sigma^{ij}$, where $\sqrt{G/g}$ denotes the deformed volume per unit undeformed volume.

One of the porous material models studied is the Gurson model (1977), in which the approximate yield condition is of the form

$$\Phi = \frac{\sigma_e^2}{\sigma_M^2} + 2q_1 f \cosh\left\{\frac{q_2}{2}\frac{\sigma_k^k}{\sigma_M}\right\} - (1 + (q_1 f)^2) = 0 \tag{3}$$

where q_1 and q_2 are adjustment factors introduced in Tvergaard (1981, 1982c), set to 1.5 and 1.0 in the present study. The macroscopic effective Mises stress is given by $\sigma_e = (3 s_{ij} s^{ij}/2)^{1/2}$ in which $s^{ij} = \sigma^{ij} - G^{ij}\sigma_k^k/3$ is the stress deviator. The Gurson model is based on the assumption that porosity exists in the form of isolated, spherical voids, and the model reduces to J_2 flow theory when $f = 0$.

Another material model used in the present study assumes that the porous aggregate consists of spherical particles bonded by isolated necks (Fleck et al., 1992). The yield surface of the FKM model is given by

$$\Phi = \left(\frac{5}{18}\frac{\sigma_e}{p_y} + \frac{2}{3}\right)^2 + \left[\frac{\sqrt{5}}{3}\frac{\frac{1}{3}\sigma_k^k}{p_y}\right]^2 - 1 = 0 \tag{4}$$

with $p_y = 2.97\sigma_M(1-f)^2\ (\hat{f}-f)/\hat{f}$ as the yield strength of the porous material under hydrostatic loading, where $\hat{f} = 0.36$.

Figure 1a shows a comparison of the FKM yield surface and that of the Gurson model. The FKM yield surface contains a vertex on the hydrostatic stress axis in $(\sigma_e, -\frac{1}{3}\sigma_k^k)$ space. For numerical computation purposes, the vertex is rounded off by a quadratic approximation to the yield surface near the vertex, as in Fleck et al. (1992).

The FKM model was developed to model the first stage of powder compaction, hence the model is appropriate at higher porosities, ranging from f well above 0.1 up to the limit of dense random packing of spherical particles, $f = 0.36$. The Gurson model is applicable at lower porosities. Thus, a combination of the two models can be made to cover a larger porosity range (Fleck et al., 1992). At porosities higher than f_1, the FKM model is used, and at porosities lower than f_2, the Gurson model is used ($f_1 > f_2$). In the transition range, $f_1 > f > f_2$, a linear combination of the two models is used

$$\Phi_{comb} = W_{fkm}\Phi_{fkm} + W_g\Phi_g = 0 \tag{5}$$

with the weight functions given by $W_{fkm} = (f-f_2)/(f_1-f_2)$ and $W_g = (f_1-f)/(f_1-f_2)$. The choice of $f_1 = 0.25$ and $f_2 = 0.1$ is made here, as in Fleck et al. (1992). Yield surfaces for the combined model at different porosities are shown in Fig. 1b.

The plastic part of the macroscopic strain increment and the effective plastic strain increment are assumed to be related by the equivalent plastic work expression

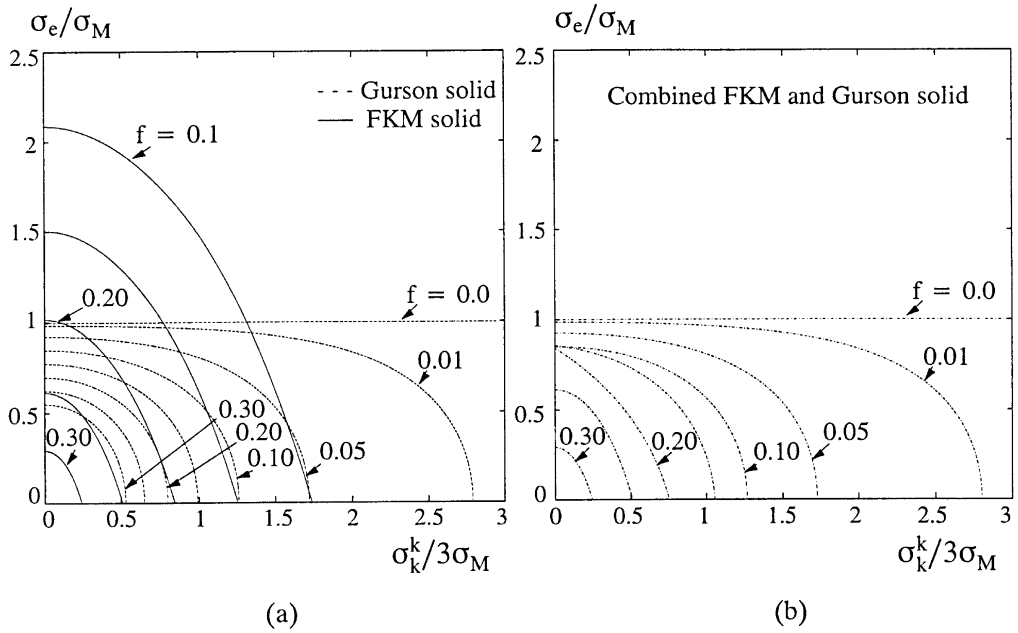

Fig. 1. Yield surface dependence on the hydrostatic pressure for various values of porosity. (a) The FKM model and the Gurson model. (b) The combined FKM and Gurson model.

$$\sigma^{ij}\dot{\eta}^{\mathrm{P}}_{ij} = F(f)\sigma_{\mathrm{M}}\dot{\varepsilon}^{\mathrm{P}}_{\mathrm{M}} \tag{6}$$

The volume fraction of deforming material in eqn (6) is given by $F = 1-f$ when the Gurson material model is used, since all of the matrix material is taken to yield. An expression for $F(f)$ in the FKM model is chosen as in Fleck et al. (1992) and is given by

$$F = \frac{45}{\sqrt{3}}(1-f)^2\left(\frac{\hat{f}-f}{\hat{f}}\right)^{3/2} \tag{7}$$

The expression for $F(f)$ in the transition range is of the same, weighted form as the yield function in eqn (5). Thus, using the uniaxial true stress natural strain curve for the matrix material

$$\dot{\varepsilon}^{\mathrm{P}}_{\mathrm{M}} = (1/E_{\mathrm{t}} - 1/E)\dot{\sigma}_{\mathrm{M}} \tag{8}$$

and the equivalent plastic work expression eqn (6), the increment of the tensile equivalent yield stress in the matrix material is obtained

$$\dot{\sigma}_{\mathrm{M}} = \frac{EE_{\mathrm{t}}}{E-E_{\mathrm{t}}}\frac{\sigma^{ij}\dot{\eta}^{\mathrm{P}}_{ij}}{F(f)\sigma_{\mathrm{M}}} \tag{9}$$

The matrix material is plastically incompressible, thus the change in porosity during an increment is approximated by

$$\dot{f} = (1-f)G^{ij}\dot{\eta}^{\mathrm{P}}_{ij} \tag{10}$$

Normality of the plastic flow is assumed

$$\dot{\eta}^{\mathrm{P}}_{ij} = \Lambda \frac{\partial \Phi}{\partial \sigma^{ij}} \tag{11}$$

The parameter, Λ, is determined from the consistency condition, $\dot{\Phi} = 0$, required during plastic loading. Then, an expression for the macroscopic plastic strain increment is derived

$$\dot{\eta}^{\mathrm{P}}_{ij} = \frac{1}{H}\frac{\partial \Phi}{\partial \sigma^{ij}}\frac{\partial \Phi}{\partial \sigma^{kl}}\overset{\triangledown}{\sigma}{}^{kl} \tag{12}$$

with

$$H = -\left(\frac{\partial \Phi}{\partial f}(1-f)G^{ij} + \frac{\partial \Phi}{\partial \sigma_{\mathrm{M}}}\frac{EE_{\mathrm{t}}}{E-E_{\mathrm{t}}}\frac{\sigma^{ij}}{F(f)\sigma_{\mathrm{M}}}\right)\frac{\partial \Phi}{\partial \sigma^{ij}} \tag{13}$$

where $(\overset{\triangledown}{})$ denotes the Jaumann derivative. Elastic unloading takes place when

$$\frac{\partial \Phi}{\partial \sigma_{kl}}\overset{\triangledown}{\sigma}{}^{kl}/H < 0.$$

The total strain increment is taken to be the sum of the elastic and plastic parts, $\dot{\eta}_{ij} = \dot{\eta}^{\mathrm{P}}_{ij} + \dot{\eta}^{\mathrm{E}}_{ij}$. Using the elastic relationship, $\overset{\triangledown}{\sigma}{}^{ij} = \mathscr{R}^{ijkl}\dot{\eta}^{\mathrm{E}}_{kl}$, the constitutive relations are obtained (e.g. see Tvergaard, 1990).

The matrix material behaviour is taken to be elastic-plastic, with the uniaxial stress strain curve approximated by the power law hardening expression

$$\varepsilon = \begin{cases} \sigma/E, & \sigma \leqslant \sigma_{\mathrm{y}} \\ \dfrac{\sigma_{\mathrm{y}}}{E}\left(\dfrac{\sigma}{\sigma_{\mathrm{y}}}\right)^{n}, & \sigma > \sigma_{\mathrm{y}} \end{cases} \tag{14}$$

where ε is the logarithmic strain, σ is the true stress, σ_{y} is the uniaxial yield stress, and n is the hardening exponent. With n very large, the material behaviour approaches that of an elastic-perfectly plastic material.

3. Localization and post-localization analysis

The model used in the present study to analyze localization of plastic flow in a shear band is shown in Fig. 2. This model has been used by a number of authors (e.g. Rice, 1976; Yamamoto 1978; Tvergaard, 1981; Saje et al., 1982) to determine the onset of localization in a homogeneously strained material. The use of the model was extended by Tvergaard (1982a) to also consider the post localization behaviour. In the analyses an initial inhomogeneity is present inside a thin slice of material and the stress-states inside and outside this slice, respectively, are assumed to remain homogeneous throughout the deformation history. The principal directions of the stresses and

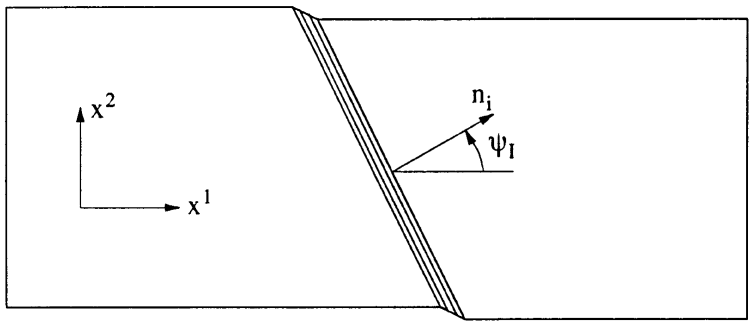

Fig. 2. Plastic flow localization in a homogeneously strained solid.

strains outside the shear band are assumed to remain fixed and parallel to the x^i-axes in the Cartesian coordinate system used as reference. The major principal stress outside the band is taken to be in the x^1-direction.

The band containing the material inhomogeneity is assumed to be parallel with the x^3-axis, and thus, in the x^1–x^2 plane, the initial orientation of the band is given by the initial angle of inclination, ψ_I, or the unit normal vector, n_i. Then, at any stage of deformation, the current angle of inclination, ψ, is obtained from

$$\tan\psi = \exp(\varepsilon_1^o - \varepsilon_2^o)\tan\psi_I \tag{15}$$

where $()^o$ denotes quantities outside the band, $()^b$ denotes quantities inside the band, and ε_i are the principal logarithmic strains. The initial void volume fractions outside and inside the band are f_I and $f_I + \Delta f$, respectively, so that the values Δf represents a material inhomogeneity.

Compatibility requires continuity of the tangential derivatives of the displacement increments, $\dot{u}_i$, over the band interface, so that the derivatives of the displacement rate components inside the band are expressed by

$$\dot{u}^b_{i,j} = \dot{u}^o_{i,j} + \dot{c}_i n_j \tag{16}$$

Here, $\dot{c}_i$ are parameters to be determined. The nominal traction on the interface inside the band must equal those outside the band so that incremental equilibrium is satisfied

$$(\dot{T}^i)^b = (\dot{T}^i)^o \tag{17}$$

where the nominal tractions on a surface with reference normal n_i are given by

$$T^i = (\tau^{ij} + \tau^{kj}u^i_{,k})n_j \tag{18}$$

Using the incremental constitutive relations and eqn (17) with $\dot{\eta}^b_{ij}$ derived from eqns (16) and (2), a set of incremental equations to determine $\dot{c}_i$ is obtained for a prescribed stress or strain history outside the band. The incremental equations can be found written out in Tvergaard (1989).

When no material inhomogeneity is present, the solution for $\dot{c}_i$ is trivial until bifurcation occurs. At the first critical bifurcation point, the governing differential equations for the three dimensional continuum loose ellipticity.

If there is a material inhomogeneity, such that the material response inside the band is softer

than that outside, the solution for $\dot{c}_i$ is non-trivial from the beginning, since the deformation state inside the band will develop faster than that outside the band. Then, the onset of localization is defined as the point where elastic unloading occurs outside the band.

It is emphasized that for a given initial orientation of the band, as specified by n_i or by the angle of inclination ψ_I, the localization analysis based on eqns (16) and (17) does not exclude prior occurrence of a singularity of the constitutive tangent operator outside or inside the band. All possible orientations have to be analysed, to find the smallest possible localization strain and the corresponding band orientation for a given imperfection amplitude. This is most clearly illustrated by the case for no material inhomogeneity, where the first singularity of the tangent operator corresponds to the band orientation giving the first bifurcation, as mentioned above, but where a choice of other band orientations will allow the analysis to go beyond the first singular point before a localization is predicted.

Both plane strain and axisymmetric analyses are carried out, by requiring

$$\varepsilon_3^o = \gamma \varepsilon_2^o \tag{19}$$

where $\gamma = 0$ gives plane strain conditions and $\gamma = 1$ results in axisymmetric behaviour. Also the effect of different stress triaxialities can be studied by using

$$\sigma_2^o = \kappa \sigma_1^o \tag{20}$$

where σ_i are the principal true stresses. Uniaxial plane strain tension or uniaxial tension, depending on γ, are obtained by setting $\kappa = 0$.

4. Results

The materials to be analysed here are specified by $\sigma_y/E = 0.0033$, $\nu = 0.3$ and $n = 10$. The porous material model used and the values of the initial porosities will be specified in each case.

The results in Fig. 3 are obtained for materials subject to uniaxial plane strain tension, $\varepsilon_3^o = 0$ and $\sigma_2^o = 0$, with the initial void volume fractions given by $f_I = 0.15$ and $\Delta f = 0.01$. The figure shows the logarithmic strain ε_1^o outside the band at localization, versus the initial angle of inclination ψ_I of the slice of material containing the inhomogeneity. Here, the onset of localization is defined as the point where elastic unloading occurs in the material outside the band.

Predictions of the three different porous material models presented in Section 2 are compared in Fig. 3. The curve predicted for the Gurson model is similar to predictions obtained for this material model in earlier publications (e.g. see Yamamoto, 1978; Tvergaard, 1981; Saje et al., 1982). Thus, the curve shows a minimum, representing the first critical localization strain for the material parameters considered, and for values of ψ_I smaller or larger than that corresponding to the minimum, the critical stain values increase rapidly. The minimum occurs at $\psi_I = 34^\circ$, which corresponds to a current angle of inclination of the band, $\psi \simeq 37^\circ$, at the onset of localization. The predictions for the FKM model are very different in that the critical strain values are very low in a wide range of ψ_I values, and in that the critical strain values vary rather little for $10^\circ < \psi_I < 40^\circ$. In fact, the strain values shown on the flat part of this FKM curve are not localizations in the usual sense, since plastic yielding never occurs outside the band, and the strain shown is the maximum value reached outside the band, slightly after the onset of yielding inside the band. The

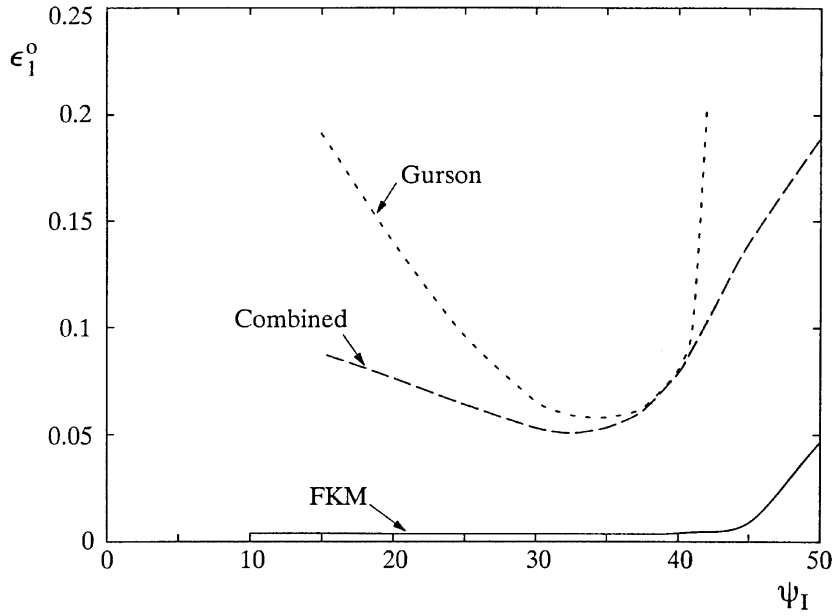

Fig. 3. Localization strain vs initial band orientation for uniaxial plane strain tension, $\varepsilon_3^o = 0$ and $\sigma_2^o = 0$. Comparing the three material models for an initial void volume fraction $f_I = 0.15$ and $\Delta f = 0.01$.

behaviour found is connected with the fact that macroscopic material softening inside the band starts soon after the onset of yielding. With this very different behaviour it should be emphasised that the FKM model is not considered very realistic at smaller values of the void volume fraction (Fleck et al., 1992), and that $f = 0.15$ is approaching the range where the FKM model should not be used at all.

The predictions for the combined model in Fig. 3 are more similar to those of the Gurson model, but still the influence of the FKM model is clearly seen in the fact that the critical strain for localization increases much more slowly as the value of ψ_I deviates from that corresponding to the minimum. In the range near the minimum, the values of the critical strains predicted for the combined model are only a little smaller than those predicted by the Gurson model. It is noted that the combined model used here, with $f_1 = 0.25$ and $f_2 = 0.10$, is the model proposed by Fleck et al. (1992) as the more realistic representation of a powder compacted metal. In the following investigations we will focus entirely on this more realistic combined model.

Figure 4 shows predictions of the combined model for different values of the initial imperfection, Δf. Here, the curve for $\Delta f = 0.01$ is identical to that shown for the combined model in Fig. 3. It is seen that there is a significant sensitivity to the value of the initial imperfection, such that the critical value of ε_1^o at the minimum for $\Delta f = 0.001$ is nearly twice as large as that at the minimum for $\Delta f = 0.01$. Localization is also predicted in the absence of imperfections, as indicated in Fig. 4 for $\Delta f = 0$. Then localization is predicted as a bifurcation from a homogeneous state of deformation (e.g. see Tvergaard, 1989). The first critical bifurcation, at the minimum of the curve for $\Delta f = 0$, represents the condition for loss of ellipticity of the governing differential equations in the uniformly strained material.

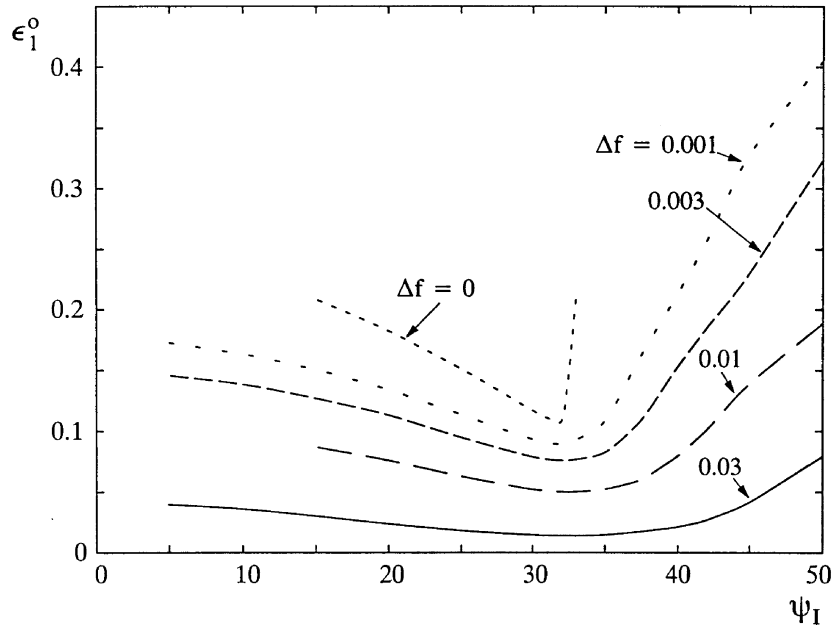

Fig. 4. Localization strain vs initial band orientation for uniaxial plane strain tension $\varepsilon_3^o = 0$ and $\sigma_2^o = 0$. Combined material model with initial void volume fraction $f_I = 0.15$ and different values of Δf.

In Fig. 5 the magnitude of the initial imperfection, $\Delta f = 0.01$, is kept constant, while three different values of f_I are considered, still for the combined model. Here, the curve for $f_I = 0.15$ was also shown in Figs 3 and 4. It is seen that the critical strain for localization increases for decreasing values of f_I. It is also seen that the curve for $f_I = 0.05$ is divided into two curves in a small range of angles, between $\psi_I = 30^\circ$ and $\psi_I = 37.5^\circ$. This means that localization is predicted when the strain reaches the value corresponding to the lower curve, but plastic yielding outside the band starts again, until secondary localization is predicted at the larger strain value corresponding to the higher curve. This is better illustrated in Fig. 6a and b for $\psi_I = 37^\circ$, which shows the development of the maximum principal strain ε^b and the void volume fraction f^b inside the band vs the maximum principal strain ε_1^o outside the band. It is seen that localization is first predicted at $\varepsilon_1^o = 0.113$, but then, when f^b reaches the value 0.10 ($=f_2$), plastic straining outside the band starts again, and the secondary onset of localization is predicted at $\varepsilon_1^o = 0.150$. Clearly, the first onset of localization is predicted while the material behaviour is entirely governed by the Gurson model, but this mode of deformation ceases soon after the combined material model is activated inside the band. To try to understand this, one needs to look at the yield surfaces for the combined model shown in Fig. 1b. It is seen that as the void volume fraction grows past the value $f_2 = 0.10$ the point where the yield surfaces cross the vertical axis, $\sigma_k^k = 0$, remains nearly fixed during a significant interval of f-values, while the direction of the yield surface normal rotates rapidly. It is clear that this significantly changes a number of terms in the equations governing localization, and the consequence is, according to the predictions in Figs 5 and 6, that further straining and void growth is needed before localization is again critical.

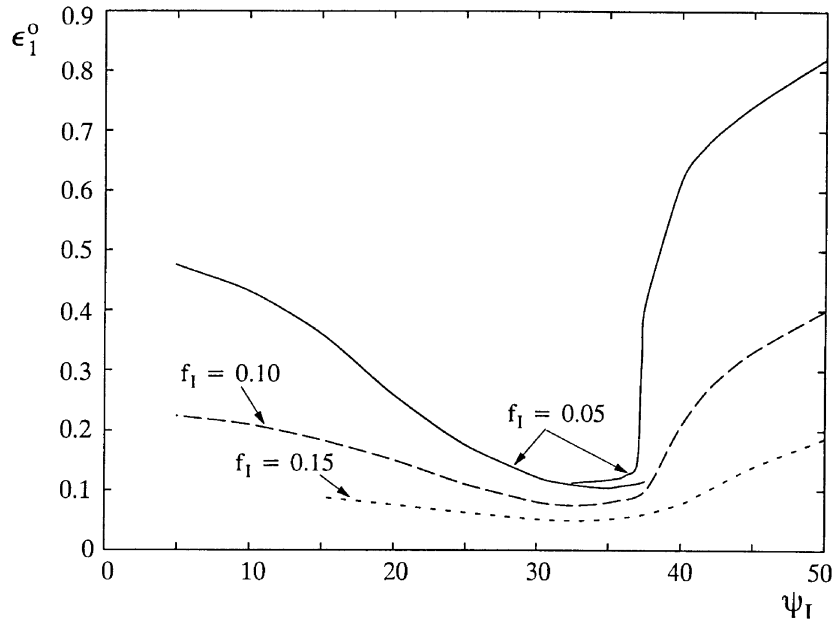

Fig. 5. Localization strain vs initial band orientation for uniaxial plane strain tension, $\varepsilon_3^o = 0$ and $\sigma_2^o = 0$. Combined material model with $\Delta f = 0.01$ and different values of f_I.

The fact that the first predicted localization does not lead to final failure in cases like that of Fig. 6, may raise some doubts regarding the importance of the predicted first critical localization. In fact, most localization studies have only shown the first critical strain. However, in the present analyses the post-localization curve has been followed a long way in all cases. Thus, it has been ensured that the subsequent mode of deformation will involve rapid void growth inside the band, with no further plastic straining outside.

In the combined model eqn (5) the values of f_1 and f_2 used here were suggested by Fleck et al. (1992). These values were not derived based on fundamental considerations, but were merely suggested as reasonable choices. Therefore, it is interesting to study the sensitivity of localization predictions to the values of these two parameters. This is done in Fig. 7 by comparing predictions for $f_2 = 0.10$ and $f_1 = 0.25$, for $f_2 = 0.14$ and $f_1 = 0.25$, and for $f_2 = 0.10$ and $f_1 = 0.21$. The curves correspond to $f_1 = 0.10$ and $\Delta f = 0.01$, so that one of the curves is identical to a curve also shown in Fig. 5. It is seen that there is rather strong sensitivity to the choice of the values f_2 and f_1 limiting the interval over which the two material models are interpolated in eqn (5). Both for an increased value of f_2 and for a reduced value of f_1 the smaller transition range results in higher minimum values of the predicted localization strain. Both changes result in more rapid rotations of the yield surface normal during the transition than those seen in Fig. 1b. In addition, there is a range of f-values, where σ_e/σ_M on the vertical axis, $\sigma_k^k = 0$, increases for increasing f. This is hardly realistic, and it therefore appears that the transition range should not be shorter than $f_1 - f_2 \simeq 0.15$. But it

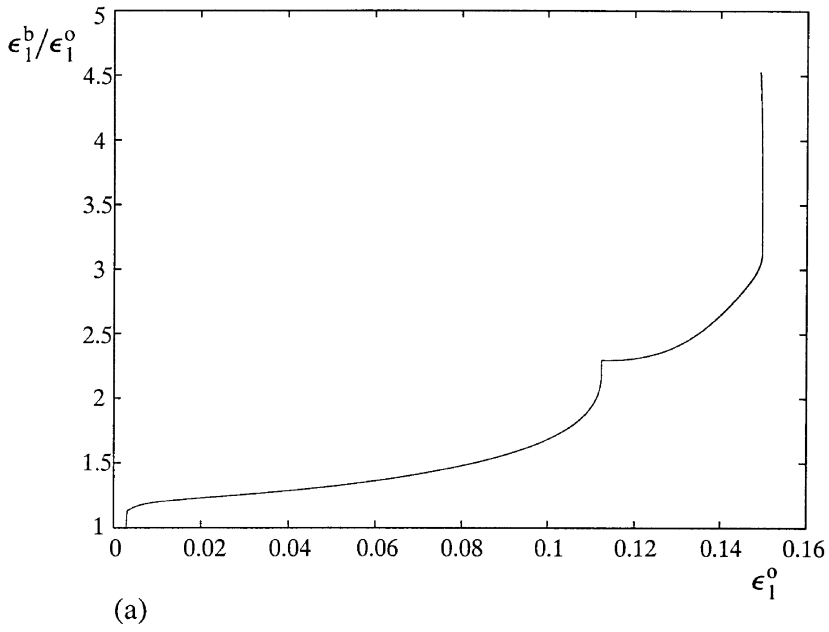

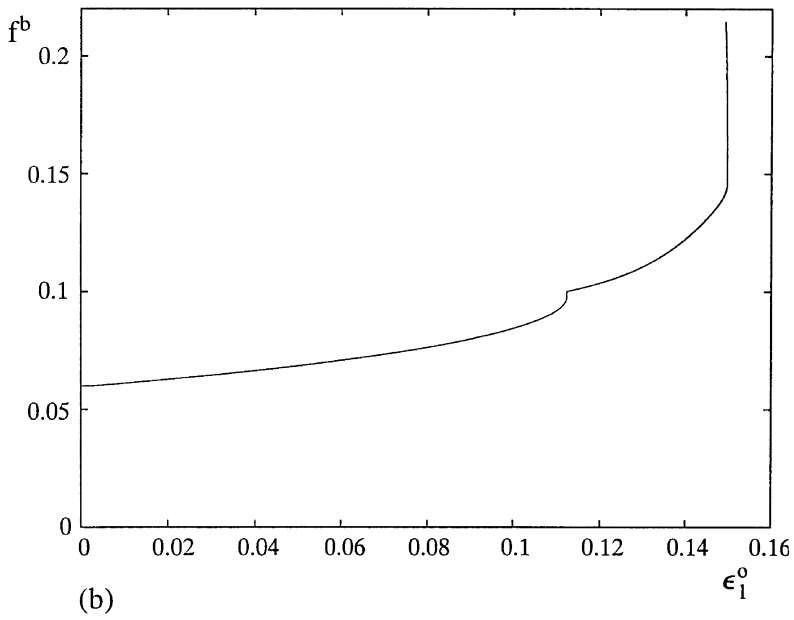

Fig. 6. Shear band development vs strain for uniaxial plane strain tension, $\varepsilon_3^o = 0$ and $\sigma_2^o = 0$, with $\psi = 37^\circ$. Combined material model with $f_I = 0.05$ and $\Delta f = 0.01$. (a) Maximum principal logarithmic stain inside band; (b) void volume fraction inside band.

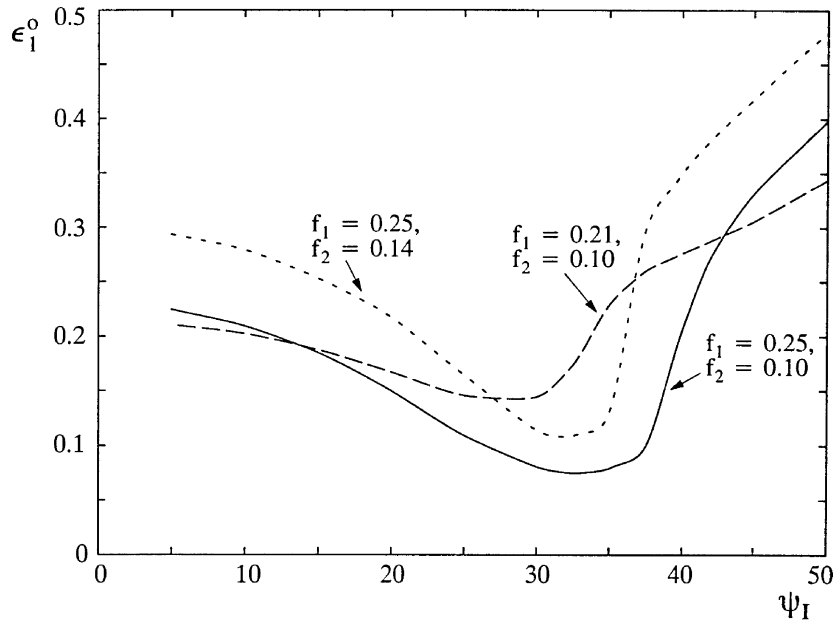

Fig. 7. Localization strain vs initial band orientation for uniaxial plane strain tension, $\varepsilon_3^o = 0$ and $\sigma_2^o = 0$. Combined material model with $f_I = 0.10$, $\Delta f = 0.01$ and different values of the parameters f_1 and f_2, defining the transition range.

is noted that the material behaviour resulting in delayed localization in Fig. 7 is similar to that resulting in the secondary localization in Fig. 6.

In Fig. 8 the effect of stress triaxiality is investigated for plane strain tension. These computations are again for the combined model with $f_2 = 0.10$ and $f_1 = 0.25$, and with the initial porosities specified by $f_I = 0.10$ and $\Delta f = 0.01$. Here, all the localization predictions are in the range where the interpolation in eqn (5) is active. Increased hydrostatic tension, as specified by $\kappa > 0$ in eqn (20), gives rise to more rapid void growth and thus earlier onset of localization. This earlier localization is seen for $\kappa = 0.25$ and $\kappa = 0.5$ in Fig. 8, for the whole range of initial band inclinations analysed.

The set of material parameters considered in Fig. 5 are also studied in Fig. 9, but now for conditions of uniaxial tension as specified by $\gamma = 1$ and $\kappa = 0$ in eqns (19) and (20). As expected for axisymmetric conditions outside the band, based on several earlier investigations for the Gurson model (e.g. see Tvergaard, 1982a, 1987), the predicted critical strains for localization are much higher than those predicted for plane strain conditions in Fig. 5. Thus, for $f_I = 0.05$ the smallest critical strain is 0.87, which is predicted for a rather small initial angle of inclination, $\psi_I = 12^\circ$. However, due to the large strains in this case the slice of material containing the higher initial porosity rotates a great deal, so that the current angle of inclination at the onset of localization is $\psi = 37^\circ$.

For axisymmetric conditions outside the band, $\gamma = 1$ in eqn (19), Fig. 10 illustrates the effect of increased stress triaxiality, analogous to the plane strain results in Fig. 8. With $f_I = 0.10$ and

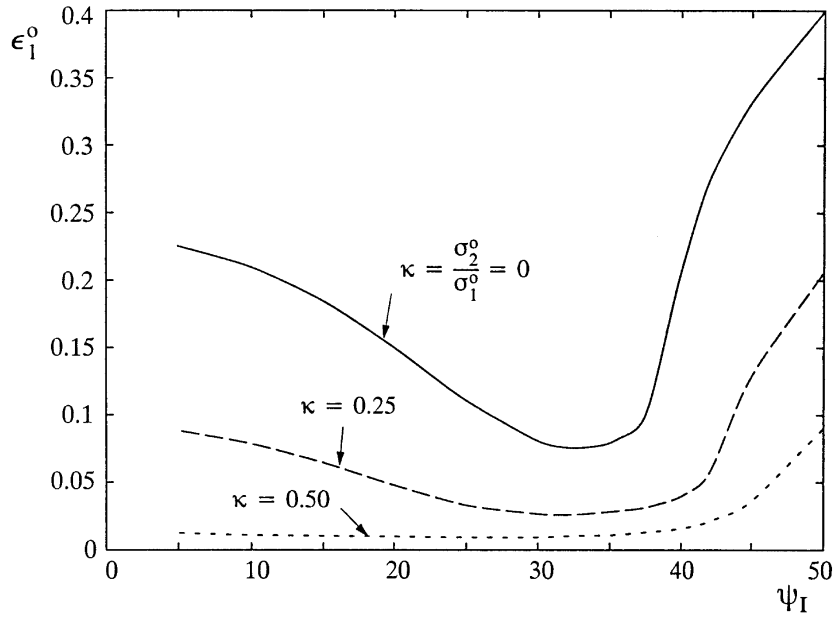

Fig. 8. Localization strain vs initial band orientation for plane strain, $\varepsilon_3^o = 0$, with different levels of transverse tension. Combined material model with $f_I = 0.10$ and $\Delta f = 0.01$.

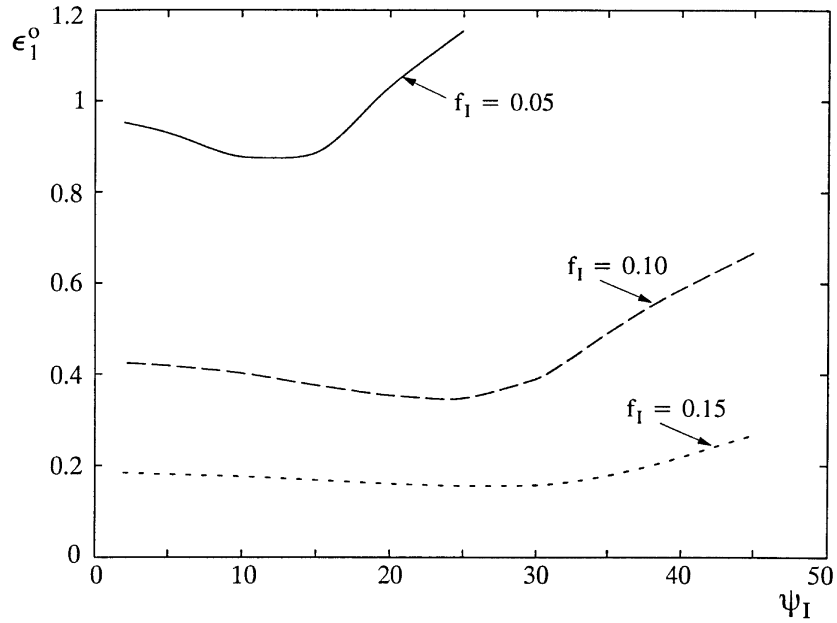

Fig. 9. Localization strain vs initial band orientation for axisymmetric uniaxial tension, $\varepsilon_3^o = \varepsilon_2^o$ and $\sigma_3^o = \sigma_2^o = 0$. Combined material model with $\Delta f = 0.01$ and different values of f_I.

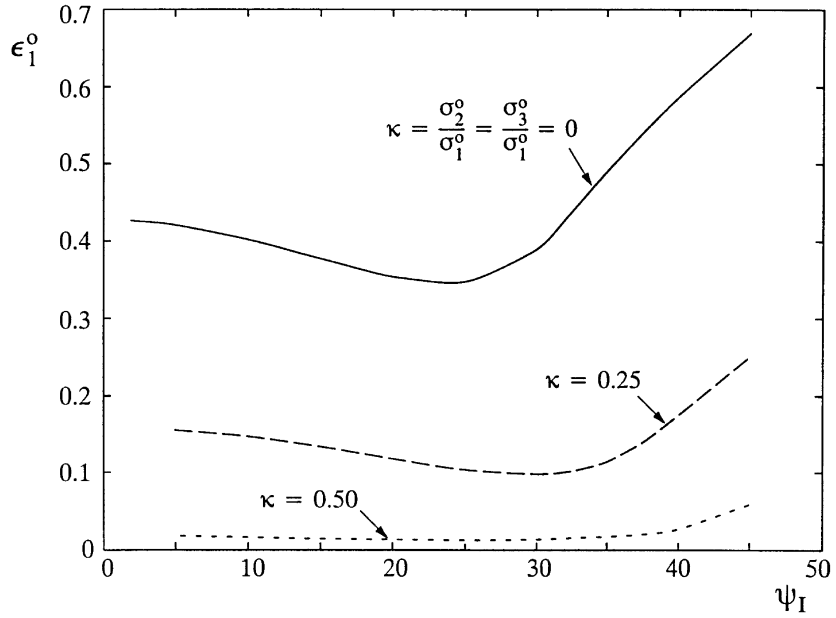

Fig. 10. Localization strain vs initial band orientation for axisymmetric conditions, $\varepsilon_3^o = \varepsilon_2^o$, with different levels of transverse tension. Combined material model with $f_I = 0.10$ and $\Delta f = 0.01$.

$\Delta f = 0.01$, the curve for $\kappa = 0$ is identical to that for $f_I = 0.10$ in Fig. 9. As in Fig. 8, the much increased rate of void growth for increased triaxiality results in earlier onset of localization, so that the curves predicted for $\kappa = 0.25$ and $\kappa = 0.50$ are much below that for $\kappa = 0$.

5. Discussion

The present results for shear localization in powder compacted materials add to the understanding already gained in a number of investigations for the Gurson model. These earlier investigations focus on rather low void volume fractions, as could result from the nucleation of voids in a dense material, whereas the present studies consider much higher initial porosities that are relevant to structural components made of sintered metals.

The new contributions in the present study relate to applications of the FKM material model for the behaviour of highly porous solids in analyses of shear band instabilities. The FKM model assumes that the porous solid consists of spherical particles bonded at isolated contacts. The microstructural morphology is expected to be appropriate at higher porosities whereas the micromechanical basis for the Gurson model, the void model, is applicable at lower porosities. Main focus in the present work has been on a combination of the two models in order to study a wide range of void volume fractions.

Since the matrix material is taken to be hardening in all the present studies, the growth in the volume fraction of porosity is the only mechanism leading to the overall softening behaviour that

results in the localization of plastic flow in shear bands. Such growth in the volume fraction of porosity requires a positive hydrostatic tension, and therefore the present investigation relates to the failure of sintered engineering components under tensile loading. During metal powder compaction this softening mechanism is not active, as the volume fraction of porosity decays, and therefore the material models considered here will not predict shear localization during compaction. A series of computations for uniaxial plane strain compression, analogous to those for tensile loading in Fig. 3, have been carried out to confirm that no shear localization is predicted by the present model under compressive loading.

The FKM model has been developed specifically for compressive loading, and it may be questioned how valid the model will be for tensile loading on sintered metals. For small changes in the volume fraction of porosity the local plastic zones in regions of contact between neighbouring metal particles will be very similar in tension and compression, assuming of course that there is full adhesion in the contact areas. As the material approaches final failure due to local necking at the contact regions, the agreement with compressive behaviour is expected to break down. Thus, for the Gurson model a significant modification, in terms of a function $f^*(f)$, was found necessary to give a reasonably accurate representation of final failure by void coalescence (Tvergaard and Needleman, 1984). Various micromechanical studies relating to the Gurson model have shown that the critical value of the void volume fraction, at which the modification $f^*(f)$ should be introduced, is of the order of 2–5 times the initial void volume fraction, with the smaller factor the larger the initial void volume fraction. Such detailed micromechanical studies of final failure have not been carried out for the FKM model. However, it is noted that in the present shear localization studies the current value of f inside the band has typically grown by a factor of 1.5 or less when the onset of localization is predicted. In this range it is expected that the FKM model will still give a reasonable approximation.

Figures 5 and 6 show the prediction of a primary flow localization, which stops growing for a while until a secondary critical strain is reached. Such behaviour has also been found by Tvergaard (1982b) in a case where a burst of stress controlled nucleation gives a brief occurrence of softening material behaviour. The same type of behaviour can occur in cases where nucleation is less sudden. Somewhat similar behaviour has also been found for a material that forms a sharp vertex on the yield surface (Hutchinson and Tvergaard, 1981) and in a study based on crystal plasticity (Tvergaard and Needleman, 1993), where initially some localized straining is predicted but then localization saturates due to a stiffening effect represented by the nonlinear constitutive model. In the present analysis the primary and secondary localizations are predicted just before and after that the void volume fractions inside the band have reached the value f_2, at which time a sharp transition to the combined regime occurs. However, even if a more smooth transition was incorporated in the material model, a similar prediction of primary and secondary flow localizations would be possible.

For the combined model, the studies in Fig. 7 have been used to investigate the sensitivity to the choice of end values f_2 and f_1 of the interpolation interval, and it has been found that the predictions are quite sensitive to this choice. The values $f_2 = 0.10$ and $f_1 = 0.25$, suggested by Fleck et al. (1992), represent a reasonable choice, which has been used in most of the present analyses. But in fact, slightly different choices could be equally reasonable.

It should be noted, finally, that all comparisons here are obtained for one particular matrix material stress-strain curve, i.e. for one particular yield strain and hardening level. Based on earlier

localization studies for the Gurson model it is expected that a more high hardening matrix material will result in delayed onset of localization, but otherwise the effect of the different parameters studied here is expected to be much the same for different levels of hardening.

Acknowledgements

The work was financially supported by the MUP2 research programme Materials Processing, Properties and Modelling, financed by the Danish Agency for Development of Trade and Industry, the Danish Natural Science Research Council and the Danish Technical Research Council.

References

Fleck, N.A., Kuhn, L.T., McMeeking, R.M., 1992. Yielding of metal powder bonded by isolated contacts. J. Mech. Phys. Solids 40, 1139–1162.

Fleck, N.A., Otoyo, H., Needleman, A., 1992. Indentation of porous solids. Int. J. Solids Structures 29(13), 1613–1636.

Gurson, A.L., 1977. Continuum theory of ductile rupture by void nucleation and growth: part I—Yield criteria and flow rules for porous ductile media. J. Engng. Materials Technol. ASME 99, 2–15.

Hutchinson, J.W., Tvergaard, V., 1981. Shear band formation in plane strain. Int. J. Solids Structures 17, 451–470.

Needleman, A., Tvergaard, V., 1987. An analysis of ductile rupture modes at a crack tip. J. Mech. Phys. Solids 35, 151–183.

Redanz, P., 1998. Numerical modelling of a cold compaction of metal powder. Int. J. Mech. Sci. 40, 1175–1189.

Redanz, P., Fleck, N.A., McMeeking, R.M., 1997. Failure of a porous solid from a deep notch. DCAMM Report 545.

Rice, J., 1976. The localization of plastic deformation. In: Koiter, W.T. (Ed.), Proceedings of the Fourteenth International Congress on Theoretical Application of Mechanics, North-Holland, Amsterdam, pp. 207–220.

Saje, M., Pan, J., Needleman, A., 1982. Void nucleation effects on shear localization in porous plastic solids. Int. J. Fracture 19, 163–182.

Tvergaard, V., 1981. Influence of voids on shear band instabilities under plane strain conditions. Int. J. Fracture 17, 389–407.

Tvergaard, V., 1982a. Material failure by void coalescence in localized shear bands. Int. J. Solids Structures 18, 659–672.

Tvergaard, V., 1982b. Influence of void nucleation on ductile shear fracture at a free surface. J. Mech. Phys. Solids 30, 399–425.

Tvergaard, V., 1982c. On localisation in ductile materials containing spherical voids. Int. J. Fracture 18, 237–252.

Tvergaard, V., 1987. Effect of yield surface curvature and void nucleation on plastic flow localization. J. Mech. Phys. Solids 35, 43–60.

Tvergaard, V., 1989. Plasticity and creep at finite strains. In: Germain, P., Piau, M., Caillerie, D. (Eds.), Theoretical and Applied Mechanics, North-Holland, pp. 349–368.

Tvergaard, V., 1990. Material failure by void growth to coalescence. In: Hutchinson, J.W., Wu, T.Y. (Eds.), Advances in Applied Mechanics Vol. 27, Academic Press, pp. 83–151.

Tvergaard, V., Needleman, A., 1984. Analysis of the cup-cone fracture in a round tensile bar. Acta Metallurgica 32, 157–169.

Tvergaard, V., Needleman, A., 1993. Shear band development in polycrystals. Proc. R. Soc. Lond. A 443, 547–562.

Tvergaard, V., van der Giessen, E., 1991. Effect of plastic spin on localization predictions for a porous ductile material. J. Mech. Phys. Solids 39, 763–781.

Yamamoto, H., 1978. Conditions for shear localization in the ductile fracture of void-containing materials. Int. J. Fracture 14, 347–365.